Metal–Organic Frameworks

DOI: 10.1002/ange.201102071

Fast Nucleation and Growth of ZIF-8 Nanocrystals Monitored by Time-Resolved In Situ Small-Angle and Wide-Angle X-Ray Scattering**

Janosch Cravillon, Christian A. Schröder, Roman Nayuk, Jeremie Gummel, Klaus Huber, and Michael Wiebcke**

Porous coordination polymers (PCPs) or metal–organic frameworks (MOFs) are a novel fascinating class of crystalline porous inorganic–organic hybrid materials, with many potential applications in gas storage, separation, sensing, catalysis, and medical diagnostics.[1] MOFs are usually synthesized from solution under mild conditions. At present, the synthesis of new MOFs is guided by choosing metal cations and polydentate organic bridging ligands with known coordination preferences that assemble with some degree of predictability into a particular three-dimensional framework,[2] which may allow further modification by post-synthetic methods.[3] One limitation of this kind of designing MOF synthesis is set by the poor understanding of the molecular-scale mechanisms of MOF crystallization.[4–6] Detailed knowledge of the physicochemical fundamentals of MOF nucleation and growth could also enable better control over crystal size and shape, an issue that is of particular relevance in the emerging field of advanced nanoscale MOF materials.[6,7] There are as yet only few experimental studies of the mechanisms of MOF crystallization. For example, ex situ extended X-ray absorption fine structure (EXAFS) spectroscopy[8] and electrospray ionization mass spectrometry (ESI-MS)[9] have been used to detect multinuclear metal complexes (secondary building units) in solution, whereas in situ static light scattering (SLS)[10] and in situ energy-dispersive X-ray diffraction (EDXRD)[5,11] have provided time-resolved information about the evolution of particles and crystalline phases, respectively. The growth of MOF nanorods by oriented attachment has also been investigated by ex situ transmission electron microscopy (TEM).[12] However, direct observations of MOF nucleation processes in homogeneous solution have as yet not been reported.

[*] J. Cravillon, C. A. Schröder, Dr. M. Wiebcke
Institut für Anorganische Chemie, Leibniz Universität Hannover
Callinstrasse 9, 30167 Hannover (Germany)
E-mail: michael.wiebcke@aci.uni-hannover.de
R. Nayuk, Prof. Dr. K. Huber
Department Chemie, Universität Paderborn
Warburger Strasse 100, 33098 Paderborn (Germany)
E-mail: klaus.huber@chemie.uni-paderborn.de
Dr. J. Gummel
European Synchrotron Radiation Facility
38043 Grenoble Cedex (France)

[**] Financial support by the DFG Priority Program 1362 "Porous Metal-Organic Frameworks" (WI1156/2-1, HU807/12-1) and provision of beam time at ID02 by ESRF is gratefully acknowledged. We thank Dr. T. Narayanan for fruitful discussions.

Supporting information for this article is available on the WWW under http://dx.doi.org/10.1002/anie.201102071.

Herein we present combined time-resolved in situ small-angle and wide-angle X-ray scattering (SAXS/WAXS) experiments that enabled for the first time monitoring the fast nucleation and growth of nanocrystals of a MOF material, the zeolitic imidazolate framework 8 (ZIF-8). Combining SAXS and WAXS is a powerful method that provides detailed information about particle size and shape and crystalline phase, as has been demonstrated previously by excellent in situ studies on the formation of zeolite,[13] $CaCO_3$,[14] Fe_3O_4,[15] and Au particles.[16]

ZIFs are a distinctive, rapidly developing subclass of MOFs.[17] Their tetrahedral framework structures consist of divalent metal cations (such as Zn^{2+}, Co^{2+}) and bridging substituted imidazolate anions, and frequently possess a zeolite topology. The prototypical ZIF-8 of composition $[Zn(mim)_2]\cdot nG$ (Hmim = 2-methylimidazole, G = guest) crystallizes with a cubic sodalite-related framework.[18] We have previously reported a procedure for the rapid production at room temperature of 45 nm sized ZIF-8 nanocrystals with a narrow size distribution.[19] An excess of the bridging Hmim ligand with respect to the zinc salt was employed to increase the nucleation rate. An in situ SLS study of the synthesis revealed that particle formation is generally characterized by comparatively slow nucleation occurring together with fast particle growth on a timescale of a few seconds, which was too fast for monitoring details of the very early crystallization events. Furthermore, SLS does not allow the detection of very small particles and crystallinity. This becomes possible by using SAXS/WAXS.

The SAXS/WAXS experiments were performed at the undulator beam line ID02 of the European Synchrotron Radiation Facility (Grenoble, France). The high brilliance of the X-ray source enabled monitoring ZIF-8 nanocrystal formation with a time resolution of 1 s. To define the onset of the fast reaction as precisely as possible, a stopped-flow device was used for rapid turbulent mixing of the methanolic component solutions before injection into a glass capillary that served as the scattering cell (experimental details are provided in the Supporting Information). The total molar ratio of $Zn(NO_3)_2\cdot 6H_2O$:Hmim:MeOH was set to 1:4:1000, in analogy to previous preparations and SLS studies employing usual mixing methods.[19]

Figure 1a and Figure 1c show plots of the experimental SAXS and WAXS patterns, respectively. Two features can be identified in the SAXS patterns. The feature of a residual intensity at the momentum transfer q of more than about $0.9\ nm^{-1}$ is already observed in the first measurement and originates from very small particles (denoted clusters hereafter); that is, these clusters form spontaneously upon mixing

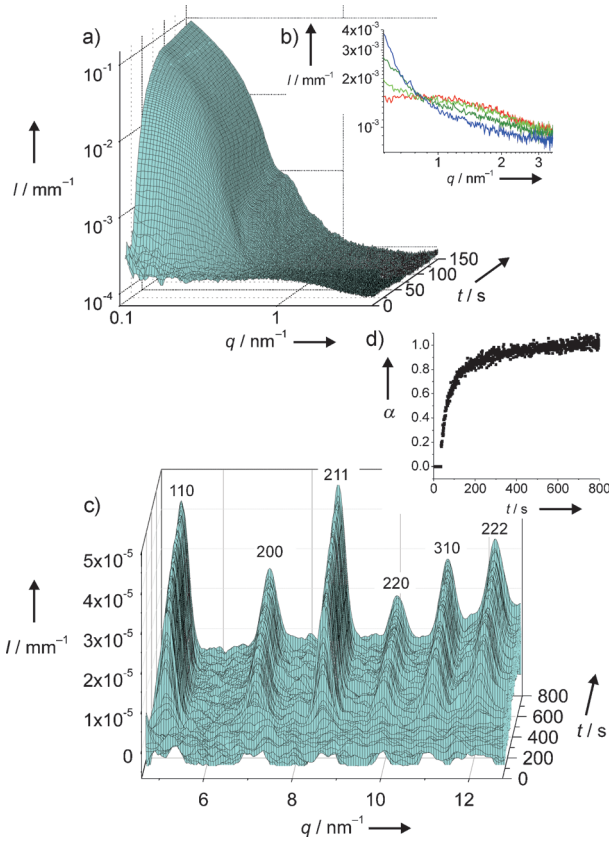

Figure 1. Time-resolved scattering patterns during ZIF-8 nanocrystal formation: a) SAXS patterns for the first 150 s. The time interval between succeeding patterns is 1 s. b) High-q region of selected SAXS patterns originating from the small particles (clusters). The time at which each pattern was measured is indicated by color: red 10 s, light green 30 s, dark green 50 s, blue 70 s. c) WAXS patterns between 1 and 800 s. The time interval between succeeding patterns is 1 s. d) Plot of the extent of crystallization α versus time t as produced from the integrated intensity of the 211 reflections in the WAXS patterns.

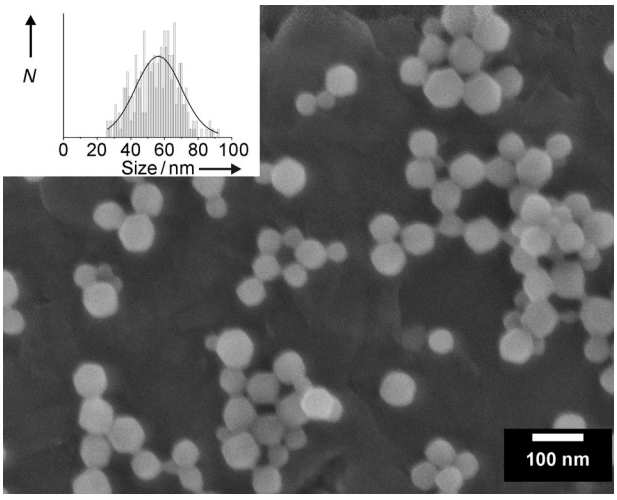

Figure 2. SEM micrograph of ZIF-8 nanocrystals obtained after turbulent mixing and 1 h reaction time. The mixing unit of a stopped-flow device was used for reproducing as close as possible the mixing conditions of the SAXS/WAXS experiments. Inset: Size distribution of the nanocrystals.

the component solutions. The feature at q less than about 0.9 nm^{-1} is first detected after 15 s and originates from the formation of particles. While the intensity corresponding to the particles increases with time, a simultaneous decrease of the intensity corresponding to the clusters is observed, indicating that the formation of particles is correlated with a depletion of clusters (Figure 1b). All Bragg reflections that appear in the WAXS patterns belong to the cubic body-centered lattice of ZIF-8 (space group $I\bar{4}3m$, $a =$ 1.7012 nm),[18a] revealing that pure-phase ZIF-8 nanocrystals are generated without the occurrence of any other transient crystalline phase.

Figure 1d shows a plot of the extent of crystallization versus time that was produced by normalization of the integrated intensity of the 211 reflections in the WAXS patterns at various times to the intensity at 800 s. The fast crystallization process slows down at about 300 s and is followed by a slower process (most likely Ostwald ripening),[19b] which may even extend beyond our last measurement at 800 s, where a maximum in intensity (and the end of reaction) has not yet been reached. A value of about 25 nm was estimated for the diameter d of the nanocrystals with an age of 800 s from the first oscillation minimum at $q \approx 0.35\ nm^{-1}$ in the SAXS pattern ($d = 4.493\,q^{-1}$).[20] A SEM micrograph (Figure 2) taken after turbulent mixing of the component solutions and 1 h reaction time reveals spherical particles with indications of a rhombic dodecahedral shape ({110} crystal form)[19] and a diameter of (55 ± 12) nm. This size is probably larger than the final size of the nanocrystals generated in the thin scattering capillary under stopped-flow conditions.

An evaluation of the SAXS data based on the Guinier approximation and the Porod invariant that is independent from any assumption of particle shape[21] has been performed after subtraction of the scattering contribution of the clusters for the period from 22 to 60 s (details of data evaluation are provided in the Supporting Information). Figure 3a and Figure 3b show the radius of gyration, weight-averaged molar mass, and number density for the particles obtained accordingly as a function of time. The increase of the values of all these parameters with time can only be interpreted with a particle growth accompanied by a continuous nucleation of new particles. Further information about the particle growth process may be obtained from the power law relation between the radius of gyration and the particle mass, $R_g \approx M_p^{\beta}$ (Figure 3c). The value of 0.35 determined for the exponent β is in close agreement with the theoretically expected value for spherical (isometric) particles of $\beta = 1/3$. A correlation of the same radii with the weight average mass of all ZIF-8 species including particles and clusters and/or small units resulted in an experimental value of 0.17. It is this division of the exponent by two that is predicted for a monomer addition mechanism.[21] Hence, particles grow by the addition of monomers (clusters and/or smaller units) but not by coalescence. This result is also in line with the increase of the

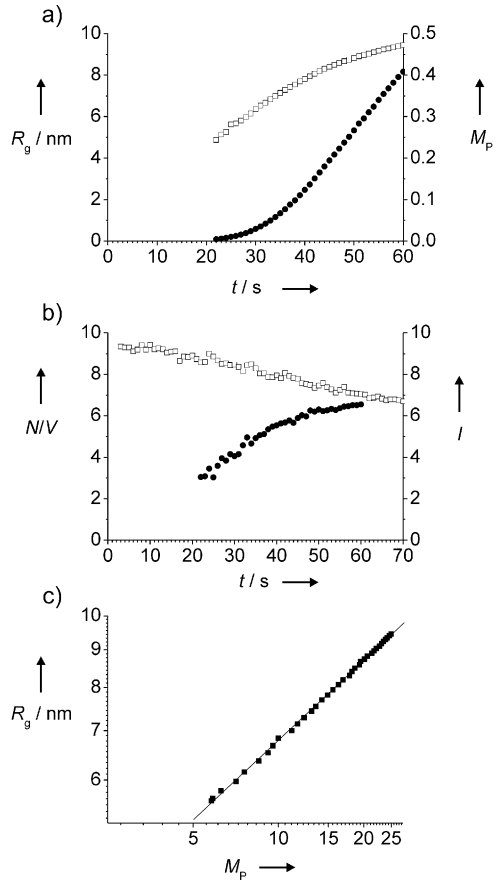

Figure 3. Parameters of ZIF-8 nanoparticles as obtained by SAXS data evaluation: a) Radius of gyration R_g and weight-averaged molar mass M_p as a function of time (□ R_g, ● M_p). b) Number density N/V of particles and scattering intensity I at $q = 1.1502\ nm^{-1}$ taken as an estimate for the mass concentration of clusters as a function of time (● N/V, □ I). c) Correlation of R_g and M_p, revealing a power-law behavior: $R_g \approx M_p^{\beta}$. The slope of the straight line gives the exponent $\beta = 0.35$.

particle number density with time, as coalescence would decrease the number density of the particles.

To further demonstrate that nucleation and/or growth of the particles occur at the expense of clusters, the mass concentration of clusters as a function of time was estimated by taking the scattering intensity at a fixed q value (Figure 3b). The intensity starts to decrease with the first observation of particles in the SAXS pattern at 15 s. At about 60 s, the clusters are nearly consumed, while the particle number density appears to approach a constant value, indicating that the nucleation process ceases by this time. At the same time, the extent of crystallization α is about 0.5 (Figure 1d). The fact that the gradual disappearance of clusters is parallel with the approach of a constant number of particles suggests that the clusters are involved in the particle nucleation process.

The SAXS patterns before the appearance of particles could be fitted with a model of monodisperse homogeneous spheres, yielding a radius for the clusters of 1.1 nm. This value should be taken as an average size estimate, as the clusters may be polydisperse. Thus, the volume of a cluster corresponds to about 1.1 unit cells of ZIF-8. After the appearance of particles, that is, after 22 s, the SAXS patterns could be fitted with a bimodal model consisting of polydisperse spheres (modeling the contribution of the particles) and monodisperse spheres or an additive Lorentzian function for random fluctuations (modeling the contribution of the clusters). Examples of model fits and the values obtained for the radius and polydispersity of the particles are provided in the Supporting Information. The values support the above model-independent data analysis.

The first point in time at which the ZIF-8 structure is established in the particles cannot be determined from the WAXS data because a few unit cells are needed for the generation of Bragg reflections and the sensitivity of WAXS is lower than that of SAXS. Thus, we cannot say whether the first particles are already crystalline or amorphous and then reorganize into the ZIF-8 structure. Extrapolation of the experimental extent of crystallization versus time (Figure 1d) to $\alpha = 0$ yields a time of about 22 s (7 s after the first appearance of particles), which may be taken as the time where the periodic ZIF-8 structure emerges.

Scheme 1 summarizes the species detected by SAXS/WAXS during the fast nucleation and growth of ZIF-8 nanocrystals under conditions of high supersaturation that are

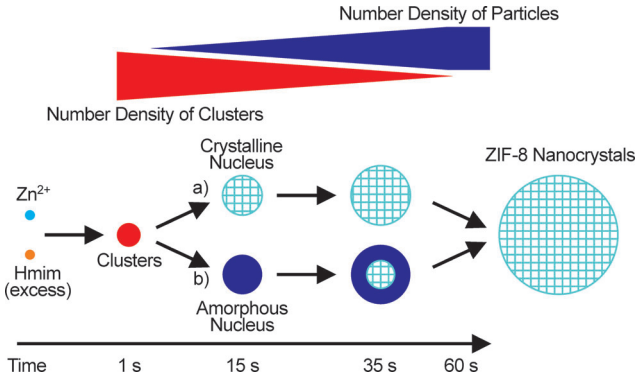

Scheme 1. Species occurring during nucleation and growth of ZIF-8 nanocrystals under conditions of high supersaturation. Two possible alternative crystallization pathways (a) and (b) are considered.

generated by the excess of the Hmim ligand. Clusters with a diameter of about 2 nm form in solution from the Zn^{2+} and Hmim precursors and transform into ZIF-8 particles. The nucleation of particles continues while the existing particles grow by attachment of monomers until the clusters are consumed. The following questions remain to be answered. First, do the clusters merely constitute a reservoir of monomers or are they actively involved in the particle nucleation process? As already mentioned, the gradual disappearance of clusters while approaching a final number of particles (Figure 3b) may support the alternative suggestion of an involvement of the clusters in nucleation. Second, if the clusters merely act as reservoir, how do the clusters contribute to the growing particles (by direct attachment and/or by dissolution into smaller building units)? Finally, if the clusters are involved in nucleation, do the clusters possess a structural

preorganization that is specific for ZIF-8 or not and by which pathway do they contribute to particle nucleation (by aggregation or growth)?

The clusters are of a similar size as the prenucleation particles that have been previously observed during the crystallization of some zeolites from clear solutions.[13,22] Strong evidence exists for an internal structural evolution towards a zeolite-related structure and aggregation of the particles during nucleation[22] and the transformation of amorphous into crystalline zeolite particles.[23] There might be similarities between ZIFs and zeolites not only in the framework topologies but also in the mechanisms of crystallization. Another question concerns the influence of the turbulent mixing. We believe that the observed ZIF-8 nanocrystal formation is valid under usual mixing conditions as well, as we have observed the same overall characteristics of the crystallization process by in situ SLS under conditions of usual mixing[19] as well as of turbulent mixing (Supporting Information, Figures S8, S9). In both cases, continuous, comparatively slow nucleation and fast crystal growth run parallel over an extended period of time.

Very recently, Venna et al.[24] reported the results of an XRD and TEM study of ZIF-8 nanocrystal formation from solutions with similar compositions (excess of Hmim) at room temperature, yet the time resolution of their ex situ experiments was too low to resolve any details of the fast crystallization process at early stages. From a classical Avrami analysis of the extent of crystallization as a function of time, they inferred that the crystallization process is nucleation-controlled and suggested the occurrence of an intermediate metastable amorphous phase. The much larger size of their nanocrystals ((230 ± 20) nm, 1 h) compared to ours may be explained by differences in experimental conditions (composition, stirring, mixing). Unfortunately, Venna et al. did not discuss the additional Bragg reflections (besides those of ZIF-8) that are clearly seen in all of their time-dependent XRD patterns. It appears likely that these additional reflections originate from an impurity phase that was generated during sample preparation for the invasive ex situ techniques, as we did not detect by our in situ experiments any other crystalline phase than ZIF-8.

In summary, we have performed in situ SAXS/WAXS investigations of a fast ZIF crystallization process with high time resolution at various length scales. This method allowed us to gain direct insight for the first time into homogeneous nucleation and early growth events. The observed prenucleation clusters and nanoparticles/nanocrystals hint at a complex crystallization process that may not follow classical nucleation theory and exhibits similarities with crystallization processes of other chemical systems, such as zeolites. It is clear that further experiments combining complementary techniques that probe different length scales, preferably under in situ conditions,[25] are needed to gain a more comprehensive picture of ZIF and MOF crystallization.

Received: March 23, 2011
Published online: July 11, 2011

Keywords: crystal growth · metal–organic frameworks · microporous materials · nanoparticles · zeolite analogues

[1] a) S. Kitagawa, R. Kitaura, S. Noro, *Angew. Chem.* **2004**, *116*, 2388; *Angew. Chem. Int. Ed.* **2004**, *43*, 2334; b) G. Férey, *Chem. Soc. Rev.* **2008**, *37*, 191.
[2] a) D. J. Tranchemontagne, J. L. Mendoza-Cortés, M. O'Keeffe, O. M. Yaghi, *Chem. Soc. Rev.* **2009**, *38*, 1257; b) J. J. Perry IV, J. A. Perman, M. J. Zaworotko, *Chem. Soc. Rev.* **2009**, *38*, 1400.
[3] Z. Wang, S. M. Cohen, *Chem. Soc. Rev.* **2011**, *40*, 498.
[4] R. E. Morris, *ChemPhysChem* **2009**, *10*, 327.
[5] F. Millange, M. I. Medina, N. Guillou, G. Férey, K. M. Golden, R. I. Walton, *Angew. Chem.* **2010**, *122*, 775; *Angew. Chem. Int. Ed.* **2010**, *49*, 763.
[6] D. Zacher, R. Schmid, C. Wöll, R. A. Fischer, *Angew. Chem.* **2011**, *123*, 184; *Angew. Chem. Int. Ed.* **2011**, *50*, 176.
[7] a) W. Lin, W. J. Rieter, K. M. L. Taylor, *Angew. Chem.* **2009**, *121*, 660; *Angew. Chem. Int. Ed.* **2009**, *48*, 650; b) A. C. McKinlay, R. E. Morris, P. Horcajada, G. Férey, R. Gref, P. Couvreur, C. Serre, *Angew. Chem.* **2010**, *122*, 6400; *Angew. Chem. Int. Ed.* **2010**, *49*, 6260.
[8] S. Surblé, F. Millange, C. Serre, G. Férey, R. I. Walton, *Chem. Commun.* **2006**, 1518.
[9] J. A. Rood, W. C. Boggess, B. C. Noll, K. W. Henderson, *J. Am. Chem. Soc.* **2007**, *129*, 13675.
[10] a) S. Hermes, T. Witte, T. Hikov, D. Zacher, S. Bahnmüller, G. Langstein, K. Huber, R. A. Fischer, *J. Am. Chem. Soc.* **2007**, *129*, 5324; b) D. Zacher, J. Liu, K. Huber, R. A. Fischer, *Chem. Commun.* **2009**, 1031.
[11] F. Millange, R. El Osta, M. E. Medina, R. I. Walton, *CrystEngComm* **2011**, *13*, 103.
[12] T. Tsuruoka, S. Furukawa, Y. Takashima, K. Yoshida, S. Isoda, S. Kitagawa, *Angew. Chem.* **2009**, *121*, 4833; *Angew. Chem. Int. Ed.* **2009**, *48*, 4739.
[13] a) P.-P. E. A. de Moor, T. P. M. Beelen, B. U. Komanschek, L. W. Beck, P. Wagner, M. E. Davis, R. A. van Santen, *Chem. Eur. J.* **1999**, *5*, 2083; b) W. Fan, M. Ogura, G. Sankar, T. Okubo, *Chem. Mater.* **2007**, *19*, 1906.
[14] a) J. Bolze, B. Peng, N. Dingenouts, P. Panine, T. Narayanan, M. Ballauff, *Langmuir* **2002**, *18*, 8364; b) D. Pontoni, J. Bolze, N. Dingenouts, T. Narayanan, M. Ballauff, *J. Phys. Chem. B* **2003**, *107*, 5123.
[15] M. Bremholm, M. Felicissimo, B. B. Iversen, *Angew. Chem.* **2009**, *121*, 4882; *Angew. Chem. Int. Ed.* **2009**, *48*, 4788.
[16] B. Abécassis, F. Testard, O. Spalla, P. Barboux, *Nano Lett.* **2007**, *7*, 1723.
[17] a) A. Phan, C. J. Doonan, F. J. Uribe-Romo, C. B. Knobler, M. O'Keeffe, O. M. Yaghi, *Acc. Chem. Res.* **2010**, *43*, 58; b) J. C. Tan, T. D. Bennett, A. K. Cheetham, *Proc. Natl. Acad. Sci. USA* **2010**, *107*, 9938; c) C. Chizallet, S. Lazare, D. Bazer-Bachi, F. Bonnier, V. Lecocq, E. Soyer, A.-A. Quoineaud, N. Bats, *J. Am. Chem. Soc.* **2010**, *132*, 12365; d) D. Esken, S. Turner, O. I. Lebedev, G. van Tendeloo, R. A. Fischer, *Chem. Mater.* **2010**, *22*, 6393; e) A. Huang, H. Bux, F. Steinbach, J. Caro, *Angew. Chem.* **2010**, *122*, 5078; *Angew. Chem. Int. Ed.* **2010**, *49*, 4958; f) T. D. Bennett, D. A. Keen, J.-C. Tan, E. R. Barney, A. L. Goodwin, A. K. Cheetham, *Angew. Chem.* **2011**, *123*, 3123; *Angew. Chem. Int. Ed.* **2011**, *50*, 3067; g) Q. Shi, Z. Chen, Z. Song, J. Li, J. Dong, *Angew. Chem.* **2011**, *123*, 698; *Angew. Chem. Int. Ed.* **2011**, *50*, 672; h) P. J. Beldon, L. Fábián, R. S. Stein, A. Thirumurugan, A. K. Cheetham, T. Friščić, *Angew. Chem.* **2010**, *122*, 9834; *Angew. Chem. Int. Ed.* **2010**, *49*, 9640; i) Y.-Q. Tian, S.-Y. Yao, D. Gu, K.-H. Cui, D.-W. Guo, G. Zhang, Z.-X. Chen, D.-Y. Zhao, *Chem. Eur. J.* **2010**, *16*, 1137.
[18] a) X.-C. Huang, Y.-Y. Lin, J.-P. Zhang, X.-M. Chen, *Angew. Chem.* **2006**, *118*, 1587; *Angew. Chem. Int. Ed.* **2006**, *45*, 1557;

b) K. S. Park, Z. Ni, A. P. Côté, J. Y. Choi, R. Huang, F. J. Uribe-Romo, H. K. Chae, M. O'Keeffe, O. M. Yaghi, *Proc. Natl. Acad. Sci. USA* **2006**, *103*, 10186.
[19] a) J. Cravillon, S. Münzer, S.-J. Lohmeier, A. Feldhoff, K. Huber, M. Wiebcke, *Chem. Mater.* **2009**, *21*, 1410; b) J. Cravillon, R. Nayuk, S. Springer, A. Feldhoff, K. Huber, M. Wiebcke, *Chem. Mater.* **2011**, *23*, 2130.
[20] O. Glatter in *Neutrons, X-rays and Light: Scattering Methods Applied to Soft Condensed Matter* (Eds.: P. Lindner, T. Zemb), North-Holland Delta Series, Amsterdam, **2002**, p. 84.
[21] J. Liu, S. Pancera, V. Boyko, A. Shukla, T. Narayanan, K. Huber, *Langmuir* **2010**, *26*, 17405.
[22] a) S. Kumar, Z. Wang, R. L. Penn, M. Tsapatsis, *J. Am. Chem. Soc.* **2008**, *130*, 17284; b) A. Aerts, M. Haouas, T. P. Caremans, L. R. A. Follens, T. S. van Erp, F. Taulelle, J. Vermant, J. A. Martens, C. E. A. Kirschhock, *Chem. Eur. J.* **2010**, *16*, 2764.
[23] S. Mintova, N. H. Olson, V. Valtchev, T. Bein, *Science* **1999**, *283*, 958.
[24] S. R. Venna, J. B. Jasinski, M. A. Carreon, *J. Am. Chem. Soc.* **2010**, *132*, 18030.
[25] N. Pienack, W. Bensch, *Angew. Chem.* **2011**, *123*, 2062; *Angew. Chem. Int. Ed.* **2011**, *50*, 2014.

